



Atomistic observation on diffusion-mediated friction between single-asperity contacts

Yang He^{1,4}, Dingshun She^{1,3,4}, Zhenyu Liu^{1,4}, Xiang Wang^{1,4}, Li Zhong¹, Chongmin Wang⁰ ^{2 ⋈}, Guofeng Wang⁰ ^{1 ⋈} and Scott X. Mao⁰ ^{1 ⋈}

The field of nanotribology has long suffered from the inability to directly observe what takes place at a sliding interface. Although techniques based on atomic force microscopy have identified many friction phenomena at the nanoscale, many interpretative pitfalls still result from the indirect or ex situ characterization of contacting surfaces. Here we combined in situ high-resolution transmission electron microscopy and atomic force microscopy measurements to provide direct real-time observations of atomic-scale interfacial structure during frictional processes and discovered the formation of a loosely packed interfacial layer between two metallic asperities that enabled a low friction under tensile stress. This finding is corroborated by molecular dynamic simulations. The loosely packed interfacial layer became an ordered layer at equilibrium distances under compressive stress, which led to a transition from a low-friction to a dissipative high-friction motion. This work directly unveils a unique role of atomic diffusion in the friction of metallic contacts.

he rapid miniaturization of nanomechanical devices raises a higher demand than ever to understand and control atomic friction between nanosized contacts¹-⁴. Previous atomic force microscope (AFM) studies and large-scale computer simulations¹-³,5,6 revealed atomic 'stick-slip' frictional behaviours, which feature a sawtooth-like friction force evolution in commensurate with the period of the substrate lattice^{7,8}. The atomic stick-slip friction is expected when the elastic constant of the AFM cantilever is lower than the curvature of the surface potential corrugation; otherwise, the scenario may convert into a regime of ultralow friction in which countermotion exhibits a continuous way with almost-zero friction⁴,9-11. This ultralow friction is crucial for improving the lifetime and efficiency of various mechanical devices.

So far, ultralow friction has been successfully demonstrated on incommensurate surfaces under conditions of low or even negative normal forces¹²⁻¹⁷. However, the atomistic mechanisms involved therein are still under extensive debate, and have been interpreted by multiple contentious theories, which include mechanical^{10,12} and thermal^{18,19} theories. For example, the transition from stick-slip to ultralow friction was interpreted by the framework of the Prandtl-Tomlinson model10,12 or as a result of the thermolubricity^{18,19}. Unfortunately, these studies focus primarily on cases in which long-range atomic diffusion is rarely involved, for example, only covalent-bonded or ionic-bonded materials are present across the interface; hence, these lubricity theories are not directly applicable to contacts that involve diffusional materials, such as metallic contacts. Lately, researchers demonstrated that the neck region mediated by atom diffusion between metallic contacts observably influences frictional behaviours²⁰⁻²². Other studies proved that neither mechanical models nor thermal contact delocalization can accurately account for the ultralow friction that occurs on Au(111) and Cu(100) surfaces, and instead conjectured that atom diffusion may be indispensable to sustain the low friction^{14,15}.

Achieving an explicit mechanistic understanding of atomic friction between diffusional metallic contacts thus requires information on the real-time interfacial structure of the contact, which is unfortunately beyond the capability of most existing experimental methods, including AFM-based techniques—the most widely applied experimental method used to study nano-/atomic-scale friction. Recent progress in in situ transmission electron microscopy (TEM) opens up a new horizon for capturing the interfacial structures during atomic friction^{21,23,24}. In the present work, by combining in situ high-resolution TEM and AFM, we successfully captured the atomic-scale frictional processes and simultaneously tracked the friction-force evolution, and we report a unique low friction behaviour between metallic contacts under tensile stress that is enabled by the formation of a loosely packed interlayer (IL) and atomic diffusion between the frictional surfaces, highlighting the critical role of interfacial structure in determining the mechanisms of atomic friction.

Figure 1 demonstrates the experimental configurations established in the present work to study atomic friction. The tip of a W probe (that is, a W single-crystal asperity) was driven by the piezosystem on a TEM holder to contact with and slide on an Au asperity deposited on an AFM cantilever (Fig. 1a-c). The mutual orientation of the asperity surfaces was precisely controlled (Fig. 1d). The friction force was calculated by Hook's law, that is, by multiplying the vertical deflection and the spring constant of the AFM cantilever. The detailed experimental procedure can be found in Methods.

Our experiments demonstrated an IL-mediated low-friction process between W and Au asperities under tensile stress (Fig. 2a–e and Supplementary Video 1). Interestingly, a loosely packed IL formed at the contact, which shows an apparently different structure and/or orientation compared to both the face-centred cubic (fcc) Au and body-centred cubic (bcc) W asperities. During friction, the structures of both the upper W and lower Au showed negligible changes, whereas the atomic contrast of the IL continuously evolved, which

¹Department of Mechanical Engineering and Materials Science, University of Pittsburgh, Pittsburgh, PA, USA. ²Environmental Molecular Sciences Laboratory, Pacific Northwest National Laboratory, Richland, WA, USA. ³Present address: School of Engineering and Technology, China University of Geosciences, Beijing, China. ⁴These authors contributed equally to this work: Yang He, Dingshun She, Zhenyu Liu, Xiang Wang. [™]e-mail: chongmin.wang@pnnl.gov; guw8@pitt.edu; sxm2@pitt.edu

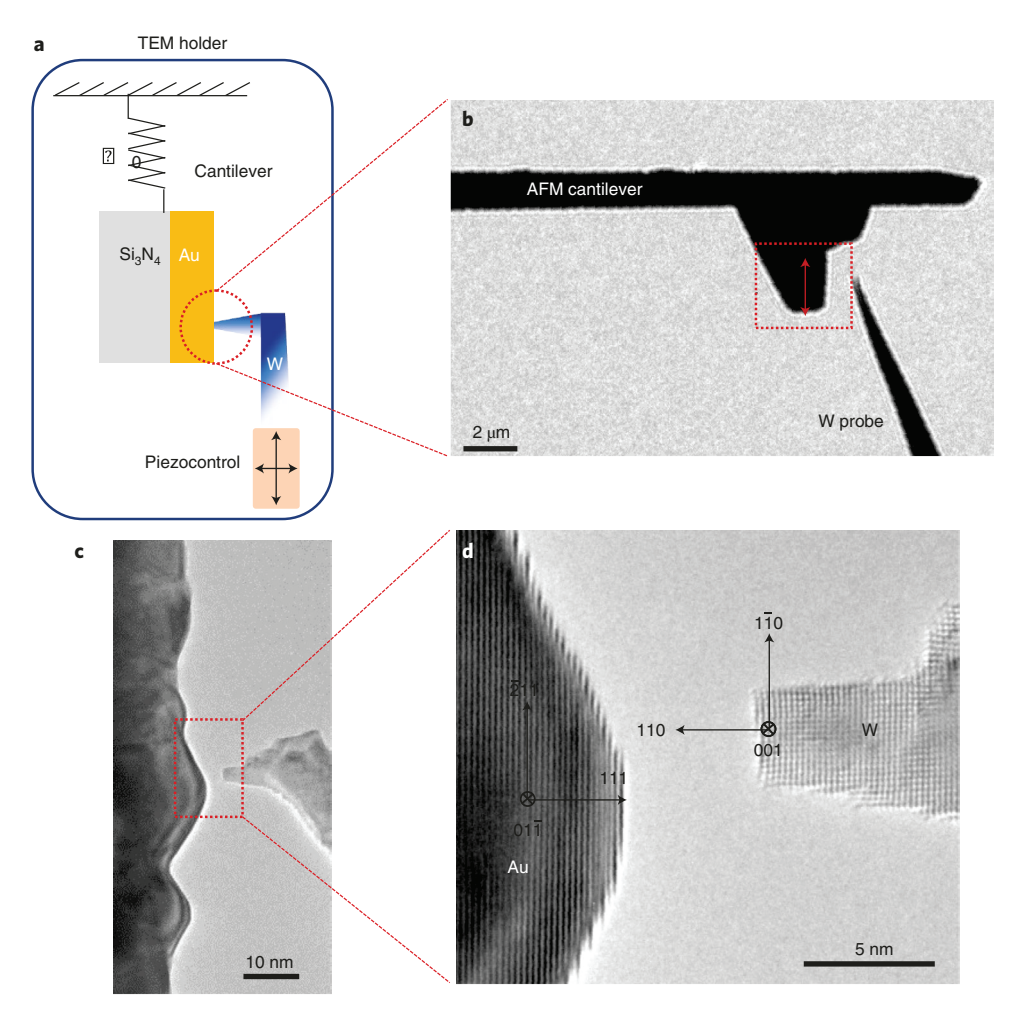


Fig. 1 | In situ TEM friction experimental set-up. a, Schematic diagram of the in situ TEM frictional experiment set-up. The tip of an AFM cantilever was reshaped and deposited with a layer of Au by ion beam sputter. The W probe (that is, the W asperity) on the counterside was manipulated to slide on the Au layer by a piezocontroller. **b**, The vertical deflection of the Au-coated AFM tip times the stiffness of the AFM cantilever gives the friction force. **c**, A close-up view of the approaching Au and W asperities. **d**, HRTEM image of the W and Au asperities on the two sides. During friction, the W probe was driven to contact and slide on the Au surface. The lateral speed of W was controlled via the piezosystem to be ~0.1 nm s⁻¹.

implies that the countermotion was primarily mediated by the IL (Fig. 2a–d). By measuring the deflection of the AFM cantilever from the sequential high-resolution transmission electron microscopy (HRTEM) images, it was found that the friction force was very low (average of $\sim 0.1\,\mathrm{nN}$) and showed slight fluctuations (Fig. 2e) during the continuous sliding²⁵. Similar experimental results that exhibit a IL-mediated low friction are presented in Supplementary Fig. 1a–j and Supplementary Video 2.

By contrast, a raised friction was observed when the loosely packed IL was absent (Fig. 2f-j and Supplementary Video 3). The Au and W asperities initially moved together along the frictional direction without relative sliding (Fig. 2f,g), which led to a gradual increase of the friction force to a maximum of ~0.8 nN—the static friction (blue dotted lines in Fig. 2j). Thereafter, the kinetic friction nearly kept constant as a lightly cyclic increase–drop evolution with the relative sliding distance between Au and W asperities. (Fig. 2g-i) The presented data deviated from the obvious saw-tooth-like fluctuation^{5,13} and the stick–slip behaviour might be hidden in the experimental results, which may ascribe to the following factors. First, the intrinsic lattice dissimilarity between Au and W interrupted the registry of commensurate contact. Second, the tensile load contributed to the reduction of the potential corrugation¹² and the ultralow scanning velocity (~0.1 nm s⁻¹) also

suppressed the fast relaxation of the lateral force^{26,27}. And last, but not least, the measurement error induced by the thermal drift and limited force resolution may dissemble the dramatic force–displacement oscillation. During the sliding process, the average friction force was ~0.7 nN, the kinetic friction (Fig. 2j), much higher than that of the case with an IL. Other cases without and with an IL were also captured by adjusting different separation distances, as shown in Supplementary Fig. 1p,q.

To understand the formation and annihilation of the loosely packed IL, molecular dynamics (MD) simulations were carried out to simulate the interfacial structure between the W and Au asperities as a function of their mutual distance (Fig. 3 and Supplementary Fig. 2). Note that Au atoms could transfer to the surface of the W asperity (Supplementary Fig. 3a–h) due to the strong Au–W adhesion^{2,28} during the friction with jump to and/or jump off contact processes, which generate saw-tooth-like clusters (Supplementary Fig. 3c,g) similar to those found in the literature²⁹. These Au clusters were metastable, and relaxed into ordered layers on the W surface (Supplementary Fig. 3h and Supplementary Video 4), which was also consistently revealed by density functional theory simulations (Supplementary Fig. 3i–o). Therefore, an Au layer with a bcc {110} (ref. ³⁰) plane structure was incorporated on the W surface in MD simulations (Supplementary Fig. 2a).

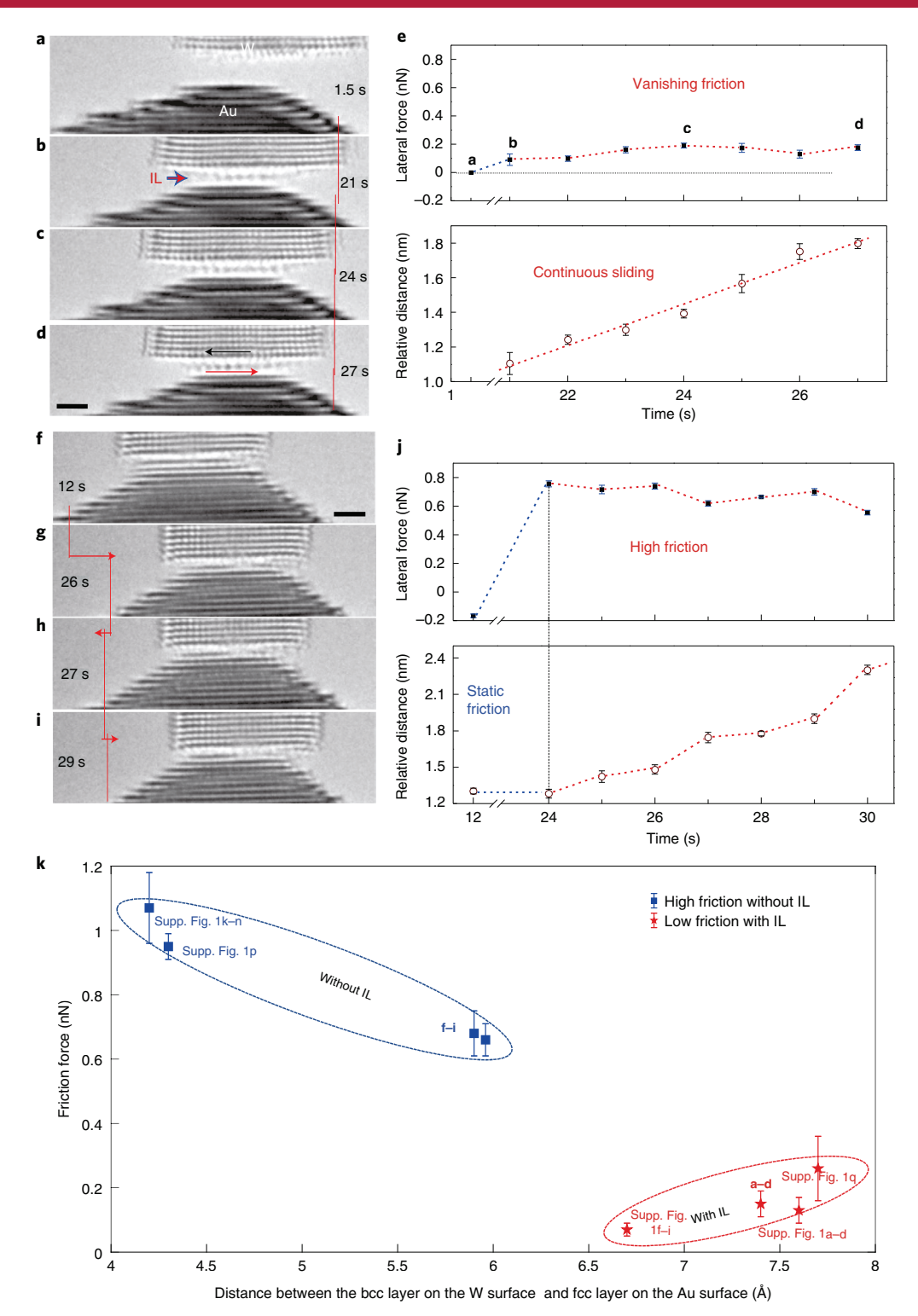


Fig. 2 | The IL induced continuous sliding with low friction compared with the high friction without an IL. a-e, Sequential HRTEM images (a-d), and friction force and relative distance evolutions with time (e, top and bottom, respectively) showing an IL-mediated low friction between W and Au asperities to give a continuous sliding with a vanishing friction force (maximum <0.2 nN). f-j, Sequential HRTEM images (f-i), and friction force and relative distance evolutions with time (j, top and bottom, respectively) showing a continuous-like sliding with a high friction between the W and Au asperities without an IL. Initially, the W and Au asperities moved together without countermotion, which manifested a static friction behaviour until the friction force reached ~0.8 nN. Then, continuous-like sliding with a high kinetic friction behaviour proceeded. The positions of the Au asperity (that is, deflection of the AFM cantilever) are marked by the red vertical lines in f-i. k, Summary of the friction behaviours with and without an IL. The error bars represent the variations of the measured friction force. Scale bars, 1 nm. Supp., Supplementary.

As shown in Fig. 3a-l, with the gradual separation of the W and Au asperities, the Au layer (as indicated by the red arrows in Fig. 3a-c) on the very interface of the bcc and fcc structures gradually

transformed into an IL wherein atoms were apparently loosely packed. Remarkably, the loosely packed IL only presented when the separation of the Au and W asperities (see Supplementary Fig. 2a

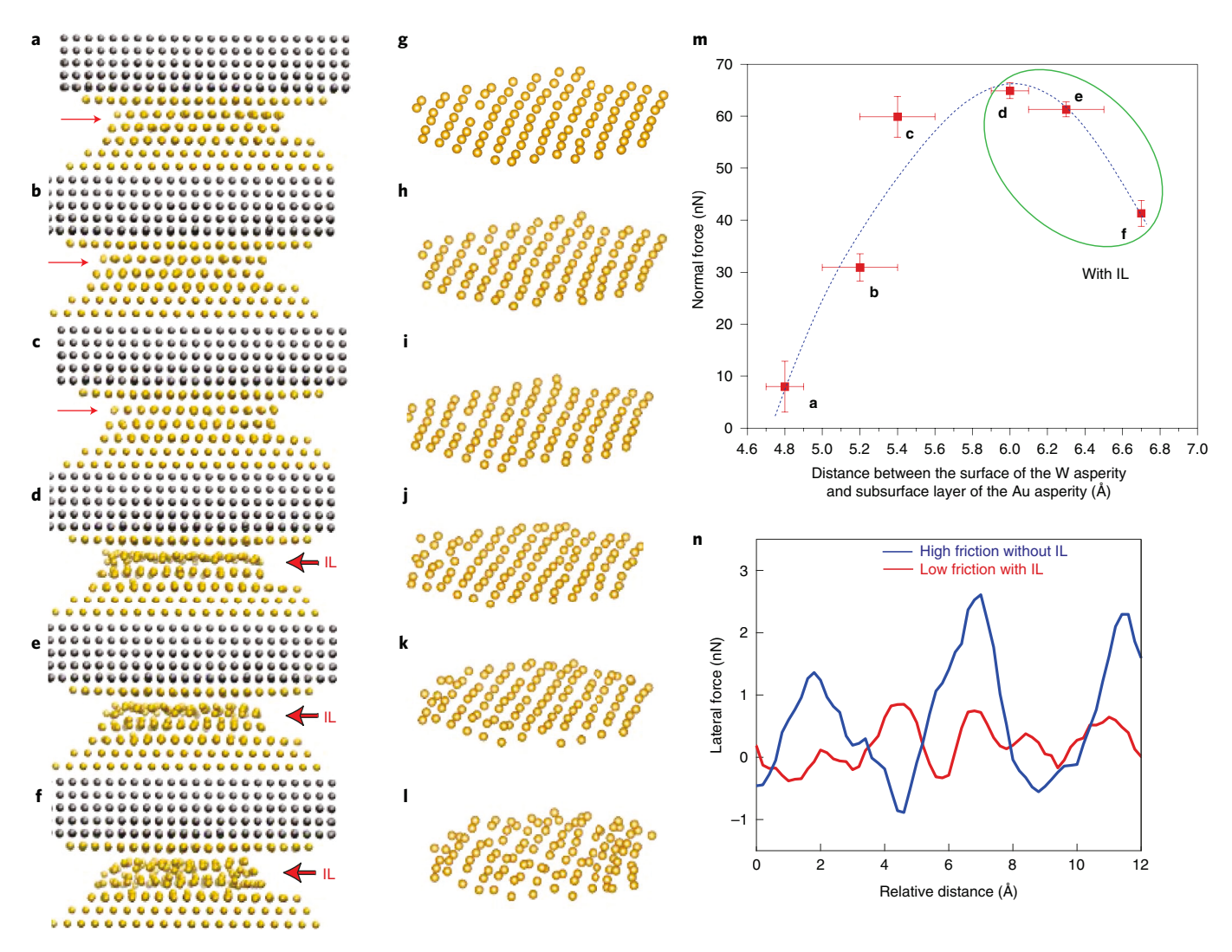


Fig. 3 | MD simulations of the interfacial structure and friction behaviour between W-Au asperities as a function of their relative distance. a-f, Simulated structures of the W and Au contact under increasing distance between the two asperities. g-I, Extracted top-layer structure of the Au asperity (indicated by the arrows), which gradually lost ordering and became loosely packed with increasing distance. **m**, Normal force evolution as a function of the distance between the bcc Au layer on the W asperity and subsurface layer of the Au asperity. The error bars represent the variations of the normal force and the distance between the surface of the W asperity and subsurface layer of the Au asperity. The dashed line is the trend line. Clearly, the loosely packed IL formed when the distance was about 6-7 Å, with the adhesion force around the maximum. **n**, Simulated friction force with and without the IL.

for the definition) reached a critical value of about 6–7 Å (Fig. 3m), which is away from the equilibrium distance (~4.7 Å including one layer of Au of ~2.35 Å). The critical dependence of the interfacial structures on the asperity distances was also consistently revealed by in situ HRTEM approaching experiments (Supplementary Fig. 2c-g). The transformation of the IL into a loosely packed structure was attributed to the competition between the Au-Au and Au-W bonding^{28,31} and the dissimilarity between the Au and W lattice for optimizing the system energy^{2,32,33}. The declining melting point and raised diffusivity of Au with decreasing the crystal size³⁴ also give rise to the possibility of this loosely packed transition. Moreover, the geometry confinement under a certain separation regime^{35,36} favoured Au clusters to relax into a monolayer structure³⁷ rather than an adhesive junction or neck^{2,21}. In addition, MD simulations (Fig. 3n) showed that atomic friction with and without the loosely packed IL exhibited a low friction force with small fluctuations (red curve) and a high friction force with large ones (blue curve), respectively, in agreement with the experimental observations shown in Fig. 2. It is worth noting that the IL only appeared at a separation distance from 6 to 7 Å when the adhesion force

between the two asperities was near the maximum value (Fig. 3m). The normal force evolution was measured as a function of the separation between the two asperities (Supplementary Fig. 4a-c). As such, the critical normal force for the IL formation was determined based on the maximum adhesion force. The friction force as a function of the separation distance in the experiments is summarized in Fig. 2k. Notably, the two regions with and without the IL exhibited distinct dependencies of the friction force on the separation distance or the normal load. Within the region without the IL, the friction force decreased with increasing separation distance or decreasing normal load (Fig. 2k and Supplementary Fig. 4d), consistent with controlling the friction behaviour by adjusting the normal load^{12,38}. For the cases with the IL, the magnitude of the friction increases slightly with decreasing the normal load within the adhesive regime (Fig. 2k and Supplementary Fig. 4d), similar to the reported scenarios with a negative friction coefficient^{30,39}, which indicated the breakdown of the Amontons' law of friction⁴⁰. The friction force underwent a sharp reduction when the IL formed, which highlights the role of an IL in determining the magnitude of the friction force.

Note that the stability of the IL is affected by the mutual orientations of the contacting surfaces of the two asperities. For example, when the contacting surfaces were not parallel, a loosely packed IL was absent under all the stress conditions or separation regimes. Instead, Au atom diffusion led to the generation of a 'neck' at the contact (Supplementary Fig. 5a,b), similar to the experimental and simulation results in the literature^{23,38,41}. The non-parallel contact broke the confinement of the atomically flat contact and created the extra space for the atom diffusion and piling up. Also, it constructed a curve configuration (Supplementary Fig. 5b) that provides an additional driving force for diffusion^{24,42}. Consequently, the countermotion was mediated by a rigid shear between the neck and Au substrate, expected to display stick–slip friction (Supplementary Fig. 5c–e).

The existence of the loosely packed IL directly lowers the static friction (Fig. 2e,j), which is similar to the structural lubricity with lattice misfit by changing the alignment conditions of the asperities to reduce the potential corrugation^{17,43}. This disorder structure enables incommensurate contact and reduces the interlocking between asperities^{9,10}, instead of the commensurate case between crystals with periodic interaction potential, which normally generates a higher friction³⁸. Owing to the high vacuum under TEM and the outstanding oxidation resistance of Au and W, the contact surface could keep clean by avoiding the interference of impurities, which provides the precondition for structural lubricity¹⁷. The IL, with the same atoms as the substrate (Au) rather than foreign atoms, has a good compliance with the substrate⁴⁴ and tends to experience a harmonically coupled deformation before sliding³⁷. Different from the absorbed fluid IL or the sliding-induced liquid phase with a certain thickness⁴⁵, the disorder monolayer also averts additional energy dissipation within the lubricant³⁷. Moreover, the tensile normal force, instead of compression⁴⁶, weakens the penetration of the IL atoms in the potential well of the substrate, analogous to controlling the normal load to lower the friction¹². Notably, compared with the case without an IL with a lower adhesive force, the loosely packed structure diluted the anchoring effect from the strong adhesion³⁹.

To further reveal the atomic mechanism inside the loosely packed IL that is responsible for ultralow kinetic friction, the dynamic evolution of the IL (Fig. 2a) during friction was analysed. As shown in the sequential HRTEM images (Fig. 4a-c) and time-resolved intensity profiles of the loosely packed IL and top Au layers (Fig. 4d and Supplementary Fig. 6), lengths of the IL and top Au layers kept evolving during friction, which indicates the severe surface diffusion of Au atoms at the vicinity of the contacting interface. Additionally, local contrasts in the IL frequently changed from strong to weak or in reverse (brown arrows in Fig. 4), which implies the mass transportation towards different directions and continuous atom rearrangements within the IL. Surface curvature and stress were reported to be important driving forces for surface diffusion at nanoscale single-asperity contacts⁴². These two driving forces kept changing during the countermotion between the Au and W asperities, and thus continuously drove atoms diffusing into or away from

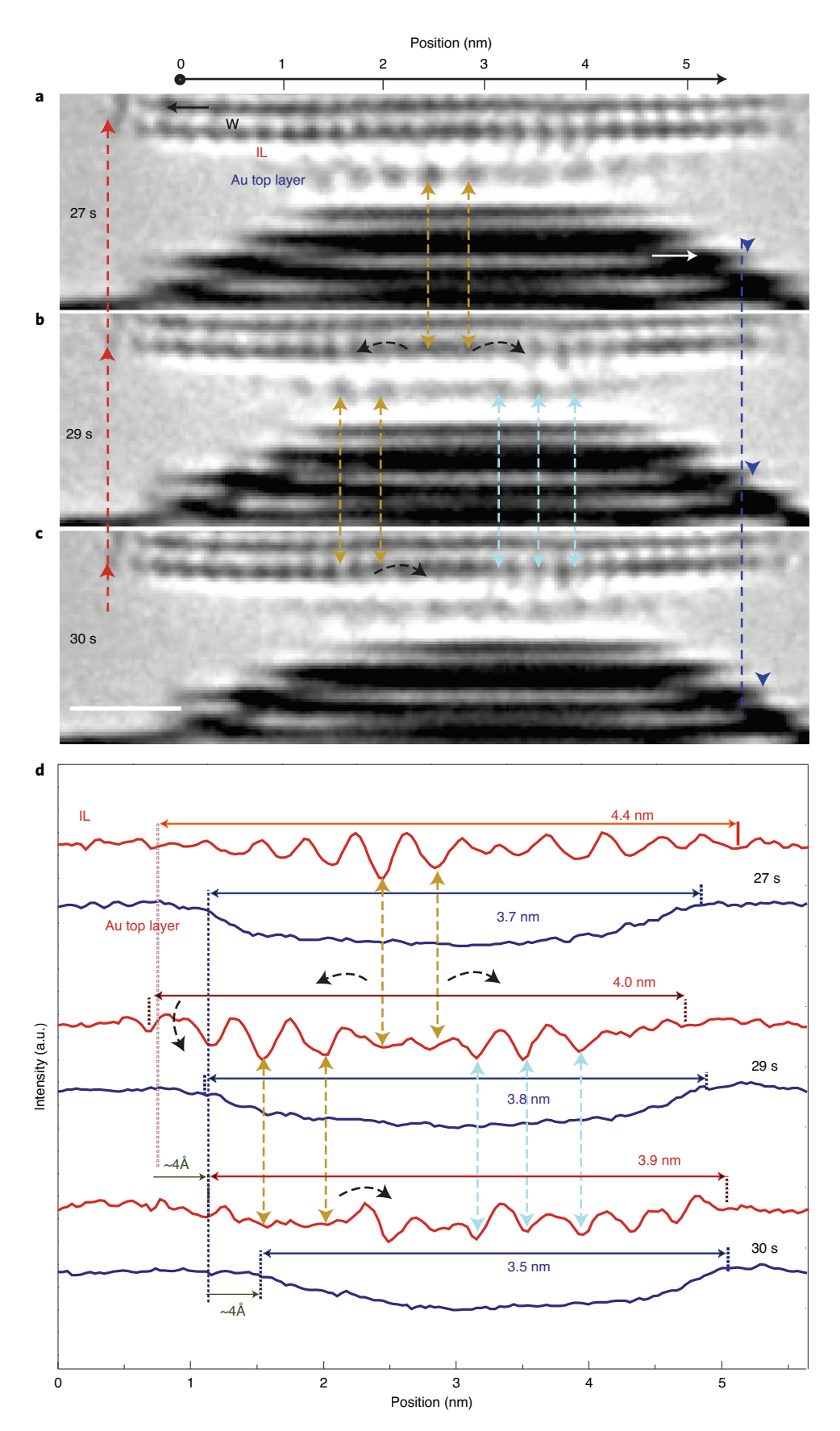
the IL. Particularly worth noting is that, as indicated by the cyan arrows in Fig. 4b-d, the local structure of the IL (as shown by the intensity features) remained sessile with respect to the W asperity during about 1-3 s, whereas the position of the IL and Au asperity moved rightwards (Fig. 4d), which implies that the migration of the IL and hence the countermotion between the Au and W asperities was mediated by atomic diffusion rather than by rigid shear, as it is in the case of high friction. To further confirm this mechanism, the dynamic evolution of the IL during friction in the MD simulation was surveyed. As shown in Supplementary Fig. 7a-i, the IL presented a disordered structure and retained the loosely packed state during the countermotion between asperities. Atoms marked by different colours within the IL (Supplementary Fig. 7a-i) experienced random jumping in different directions and exhibited various motion pathways, contrary to the uniform movement assisted by the interface dislocation slipping^{47,48}. The mean square displacement of the interface and reference layers of Au atoms in the case with an IL during friction in the MD simulation was calculated, as shown in Supplementary Fig. 7m. The mean square displacement of the IL atoms increased sublinearly with time, much higher than that of the reference layer, which indicates that random diffusion activities dominated the motion of the IL atoms^{42,49}. The mean square displacement in the reference layer, however, was limited and mainly from the contribution of the elastic displacement of atoms driven by the suffered shear stress. The loosely packed IL simply went through a diffusive mass flow instead of the periodic crystallization and melting process^{33,50}, which generated extra energy dissipation⁵¹. As a result, these observations demonstrate that the low friction behaviour observed in Fig. 2 is mediated by the loosely packed IL via vigorous diffusive activities near the contact. This IL played a similar role as a self-lubricity that mediates the countermotion between asperities. Atomic friction in our experiments carried out between incommensurate interfaces under a slow countermotional speed of 10^{-10} m s⁻¹ and low normal loads prompted thermolubricity and can effectively reduce surface energy corrugation^{4,6,9-11,15,18,19,25}. The direct observation of a loosely packed IL at the contacting interface and noteworthy atomic diffusion involved therein indicates that the underlying mechanism of low friction at contacts that involve diffusional metals is more complex than previous simple rigid sliding interpretations^{7,52}. The geometry confinement designed here also suppressed the formation of a junction induced by diffusion, which differs from the scenario dominated by the yielding and fracture of a junction with high resistance^{2,15}. The mean interfacial shear stress in the friction experiment was estimated, as summarized in Supplementary Table 2. The contact with the IL displayed a lower interfacial shear strength compared with that with an ordered IL, which was attributed to the loosely packed interfacial structure and the diffusion-mediated countermotion during friction. The unique structure characters of the IL and associated loading conditions determine the role of a diffusive IL on the friction, which provides insights into the selection of lubricity.

It has been reported that surface atom diffusion contributes substantially to the mechanical behaviours of nanosized crystals^{29,53–55}.

Fig. 4 | Low friction mediated by atomic diffusion in the loosely packed IL. a-d, Sequential HRTEM images (**a-c**) and intensity profiles of the IL and top layer of the Au asperity (**d**). The red and blue arrow heads indicate the reference points on the W and Au asperities. The red dashed line indicates that the images are aligned based on the position of the W asperity. The blue dashed line and arrows indicate that the Au asperity migrated rightwards with respect to the W asperity. The length and position of the IL (as labelled in **d**) were identified by matching the intensity profile with the corresponding HRTEM images. The length and position of the Au top layer were measured from the intensity profile by assuming the edge of the Au layer was at the upper end of the intensity slope. The lengths of the IL and Au layer varied during friction, which provides strong evidence of atom diffusion into or away from the edges of the IL and Au layer. As indicated by the brown arrows, local contrasts in the IL frequently changed from strong to weak or in reverse, which implies continuous atom rearrangements as a result of diffusion. The diffusion flow is indicated by the black dash arrows. Cyan arrows indicate local intensity features that remained sessile in the IL for about 1–3 s with respect to the W asperity; however, the position of the IL and Au asperity moved rightwards during the period (horizontal black arrows in **d**). Scale bar, 1 nm. a.u., arbitrary units.

Metals with large diffusivity, such as Au and Ag, even exhibit a 'liquid-like' behaviour at the lower nanoscale 54,55 . Jaklevic and Elie reported that it takes only $\sim 0.12 \, \mathrm{s}$ for gold atoms to diffuse from

one atomic site to another (~0.23 nm) under ambient temperature⁵³, which is much faster compared with the sliding speed in our experiments. The diffusivity of metals also increases with decreasing the



sample and/or device's size³⁴. These previous results rationalize our observation of diffusion during atomic friction (Fig. 4). Given sufficient time, driving force and space, the atomic diffusion makes the IL liquid-like during friction. The diffusion can also be activated by tribo-induced heating⁴⁵ or at high temperatures. As such, it is reasonable to expect the IL and ensuing diffusion-mediated low friction behaviour may widely exist in the broad class of nanoscale metallic contacts.

Additionally, this work provides a direct atomic-scale observation of the real-time microstructure of the interface during friction, and could thus serve as a paradigm for studying atomic friction. Under tensile stress, a loosely packed IL is formed by atom diffusion, which serves as a lubricant between the countersliding asperities and results in an ultralow friction. The IL only exists at the distance of the highest adhesive stress and disappears when approaching the equilibrium distance. Besides, the contact angle of the asperity surfaces also plays a non-negligible role in the interfacial structure, and thereby influences the basic mechanism of atomic friction. Our work unravels an origin for the low friction between metallic single asperities that are beyond the general expectation, which highlights the critical role of atom diffusion in determining the interfacial structure and hence the atomic mechanisms of friction.

Online content

Any methods, additional references, Nature Research reporting summaries, source data, extended data, supplementary information, acknowledgements, peer review information; details of author contributions and competing interests; and statements of data and code availability are available at https://doi.org/10.1038/s41563-021-01091-3.

Received: 4 December 2020; Accepted: 28 July 2021; Published online: 7 October 2021

References

- 1. Carpick, R. W. Controlling friction. Science 313, 184-185 (2006).
- Landman, U., Luedtke, W., Burnham, N. A. & Colton, R. J. Atomistic mechanisms and dynamics of adhesion, nanoindentation, and fracture. *Science* 248, 454–461 (1990).
- Bhushan B. Nanotribology and Nanomechanics: An Introduction (Springer Science & Business Media. 2008).
- Lantz, M. A., Wiesmann, D. & Gotsmann, B. Dynamic superlubricity and the elimination of wear on the nanoscale. *Nat. Nanotechnol.* 4, 586–591 (2009).
- Mate, C. M., McClelland, G. M., Erlandsson, R. & Chiang, S. in Scanning Tunneling Microscopy (ed. Neddermeyer, H.) 226–229 (Springer, 1987).
- Dong, Y., Li, Q. & Martini, A. Molecular dynamics simulation of atomic friction: a review and guide. J. Vac. Sci. Technol. A 31, 030801 (2013).
- Tomlinson, G. J. T. L. A molecular theory of friction. Lond. Edinb. Dublin Phil. Mag. J. Sci. 7, 905–939 (1929).
- Weiss, M. & Elmer, F.-J. Dry friction in the Frenkel-Kontorova-Tomlinson model: static properties. *Phys. Rev. B* 53, 7539–7549 (1996).
- Shinjo, K. & Hirano, M. Dynamics of friction: superlubric state. Surf. Sci. 283, 473–478 (1993).
- Hölscher, H., Schirmeisen, A. & Schwarz, U. D. Principles of atomic friction: from sticking atoms to superlubric sliding. *Phil. Trans. R. Soc. A* 366, 1383–1404 (2008).
- Kim, W. K. & Falk, M. L. Atomic-scale simulations on the sliding of incommensurate surfaces: the breakdown of superlubricity. *Phys. Rev. B* 80, 235428 (2009).
- Socoliuc, A., Bennewitz, R., Gnecco, E. & Meyer, E. Transition from stick-slip to continuous sliding in atomic friction: entering a new regime of ultralow friction. *Phys. Rev. Lett.* 92, 134301 (2004).
- Bennewitz, R. et al. Atomic-scale stick-slip processes on Cu(111). Phys. Rev. B 60, R11301-R11304 (1999).
- Gosvami, N. N., Filleter, T., Egberts, P. & Bennewitz, R. Microscopic friction studies on metal surfaces. *Tribol. Lett.* 39, 19–24 (2010).
- Bennewitz, R., Hausen, F. & Gosvami, N. N. Nanotribology of clean and modified gold surfaces. J. Mater. Res. 28, 1279–1288 (2013).
- Socoliuc, A. et al. Atomic-scale control friction by actuation of nanometer-sized contacts. Science 313, 207–210 (2006).

 Dietzel, D., Schwarz, U. D. & Schirmeisen, A. Nanotribological studies using nanoparticle manipulation: principles and application to structural lubricity. *Friction* 2, 114–139 (2014).

- Krylov, S. Y., Dijksman, J., Van Loo, W. & Frenken, J. Stick-slip motion in spite of a slippery contact: do we get what we see in atomic friction? *Phys. Rev. Lett.* 97, 166103 (2006).
- Krylov, S. Y. & Frenken, J. W. Thermal contact delocalization in atomic scale friction: a multitude of friction regimes. New J. Phys. 9, 398–423 (2007).
- Liao, Y. & Marks, L. In situ single asperity wear at the nanometre scale. Int. Mater. Rev. 62, 99–115 (2017).
- Sato, T., Ishida, T., Jalabert, L. & Fujita, H. Real-time transmission electron microscope observation of nanofriction at a single Ag asperity. *Nanotechnology* 23, 505701 (2012).
- Ishida, T. et al. Time-lapse nanoscopy of friction in the non-Amontons and non-Coulomb regime. Nano Lett. 15, 1476–1480 (2015).
- Fujisawa, S. & Kizuka, T. Lateral displacement of an AFM tip observed by in-situ TEM/AFM combined microscopy: the effect of the friction in AFM. *Tribol. Lett.* 15, 163–168 (2003).
- Zhong, L. et al. Slip-activated surface creep with room-temperature super-elongation in metallic nanocrystals. Nat. Mater. 16, 439–445 (2017).
- Hirano, M. Superlubricity: a state of vanishing friction. Wear 254, 932–940 (2003).
- Gnecco, E. et al. Velocity dependence of atomic friction. Phys Rev. Lett. 84, 1172–1175 (2000).
- Breki, A. & Nosonovsky, M. Ultraslow frictional sliding and the stick-slip transition. *Appl. Phys. Lett.* 113, 241602 (2018).
- Oliver, D. et al. One-to-one spatially matched experiment and atomistic simulations of nanometre-scale indentation. *Nanotechnology* 25, 025701 (2013).
- Schaefer, D., Patil, A., Andres, R. & Reifenberger, R. Elastic properties of individual nanometer-size supported gold clusters. *Phys. Rev. B* 51, 5322–5332 (1995).
- Thormann, E. Negative friction coefficients. Nat. Mater. 12, 468–468 (2013).
- Oliver, D. et al. Conductivity of an atomically defined metallic interface. Proc. Natl Acad. Sci. USA 109, 19097–19102 (2012).
- Vitos, L., Ruban, A., Skriver, H. L. & Kollar, J. The surface energy of metals. Surf. Sci. 411, 186–202 (1998).
- Bhushan, B., Israelachvili, J. N. & Landman, U. J. N. Nanotribology: friction, wear and lubrication at the atomic scale. *Nature* 374, 607–616 (1995).
- Dick, K., Dhanasekaran, T., Zhang, Z. & Meisel, D. Size-dependent melting of silica-encapsulated gold nanoparticles. *J. Am. Chem. Soc.* 124, 2312–2317 (2002).
- Luedtke, W. & Landman, U. Solid and liquid junctions. Comput. Mater. Sci. 1, 1–24 (1992).
- Karaborni, S. Order-disorder transition during approach and separation of two parallel surfaces. Phys. Rev. Lett. 73, 1668–1671 (1994).
- Cieplak, M., Smith, E. D. & Robbins, M. O. Molecular origins of friction: the force on adsorbed layers. Science 265, 1209–1212 (1994).
- So, M., Jacobsen, K. W. & Stoltze, P. Simulations of atomic-scale sliding friction. Phys. Rev. B 53, 2101–2113 (1996).
- Deng, Z., Smolyanitsky, A., Li, Q., Feng, X.-Q. & Cannara, R. J. Adhesion-dependent negative friction coefficient on chemically modified graphite at the nanoscale. *Nat. Mater.* 11, 1032–1037 (2012).
- Amontons, G. De la resistance cause'e dans les machines (About resistance and force in machines). Mem l'Aced. R. 1699, 257–282 (1699).
- Merkle, A. P. & Marks, L. D. Liquid-like tribology of gold studied by in situ TEM. Wear 265, 1864–1869 (2008).
- Guo, W., Wang, Z. & Li, J. Diffusive versus displacive contact plasticity of nanoscale asperities: temperature- and velocity-dependent strongest size. *Nano Lett.* 15, 6582–6585 (2015).
- Hirano, M., Shinjo, K., Kaneko, R. & Murata, Y. Anisotropy of frictional forces in muscovite mica. *Phys. Rev. Lett.* 67, 2642–2645 (1991).
- He, G., Müser, M. H. & Robbins, M. O. Adsorbed layers and the origin of static friction. Science 284, 1650–1652 (1999).
- Dawson, B., Lee, S. & Krim, J. Tribo-induced melting transition at a sliding asperity contact. *Phys. Rev. Lett.* 103, 205502 (2009).
- Müser, M. H., Wenning, L. & Robbins, M. O. Simple microscopic theory of Amontons's laws for static friction. *Phys. Rev. Lett.* 86, 1295–1298 (2001).
- Hurtado, J. A. & Kim, K. S. Scale effects in friction of single–asperity contacts. I. From concurrent slip to single–dislocation–assisted slip. *Proc. R. Soc. Lond. A* 455, 3363–3384 (1999).
- Dong, Y., Li, Q., Wu, J. & Martini, A. Friction, slip and structural inhomogeneity of the buried interface. *Model. Simul. Mater. Sci. Eng.* 19, 065003 (2011).
- Tanaka, M. Molecular dynamics study of velocity autocorrelation function in a model of expanded liquid rubidium. *Prog. Theor. Phys. Suppl.* 69, 439–450 (1980).

- Yoshizawa, H., McGuiggan, P. & Israelachvili, J. Identification of a second dynamic state during stick-slip motion. *Science* 259, 1305–1308 (1993).
- Thompson, P. A. & Robbins, M. O. Origin of stick-slip motion in boundary lubrication. *Science* 250, 792–794 (1990).
- 52. Müser, M. H. Velocity dependence of kinetic friction in the Prandtl–Tomlinson model. *Phys. Rev. B* **84**, 125419 (2011).
- Jaklevic, R. & Elie, L. Scanning-tunneling-microscope observation of surface diffusion on an atomic scale: Au on Au(111). Phys. Rev. Lett. 60, 120–123 (1988).
- Gu, X. W. et al. Pseudoelasticity large strains Au nanocrystals. *Phys. Sci. Rev.* 121, 056102 (2018).
- Sun, J. et al. Liquid-like pseudoelasticity of sub-10-nm crystalline silver particles. Nat. Mater. 13, 1007–1012 (2014).

Publisher's note Springer Nature remains neutral with regard to jurisdictional claims in published maps and institutional affiliations.

© The Author(s), under exclusive licence to Springer Nature Limited 2021

Methods

Au–AFM cantilever preparation. The AFM cantilever with Au crystals on top was prepared sequentially, as follows:

- Commercially available AFM cantilevers from Bruker AFM Probes were
 used in this investigation. The 'F' MSCT cantilever was used, with a spring
 constant of ~0.6 N m⁻¹ and a triangular geometry; both the tip and cantilever
 were made of silicon nitride and came with an Au coating on the back side.
 The spring constant of the cantilever was precisely measured by using an
 AFM before subsequent processing.
- 2. The cantilever was machined by using a focus ion beam (FIB; FEI-Helios). The back of the AFM chip was pasted onto a scanning electron microscope stage which was loaded into the FIB. For the first step, the tip of the cantilever was machined flat (Supplementary Fig. 8a–c). Then, the AFM chip was taken out of the scanning electron microscope stage, rotated 90° and pasted back onto the stage; the tip now faced upwards (Supplementary Fig. 8d). In the second step, the tip was machined from the top into a wedge shape with a side surface inclination angle of ~38° (Supplementary Fig. 8e). The final thickness of the wedge tip ('edge') was ~20 nm. The wedge-shaped tip provided two crucial characteristics for the friction tests: the mechanical stability during friction and the electron transparency of the deposited Au. The FIB processing may induce the Ga residual into Au crystals.
- After reshaping the cantilever tip with FIB, the AFM chip was transferred into an ion-beam sputter for Au deposition. An Au target with a 99.9 wt% purity was used for the deposition. Note that a small amount (<5 at%) of Al was doped into the deposited Au, due to the deficiency of the ion-beam sputter. An 'electron-beam shower' inside the TEM was applied to the Au tip to sufficiently sputter Al atoms off the sample before the friction experiments. Owing to the lower melting point of Ga compared to that of Al, the Ga residual can be sputtered off together with Al atoms under the electron-beam shower. The impurity interruption induced by the FIB preparation can be eliminated. The deposition was targeted on the edge of the wedged tip (that is, along the viewing direction in Supplementary Fig. 8e), and a total amount of ~20 nm Au was deposited. The deposited Au formed a polycrystalline dense film with almost flat surfaces on the edge of the wedged tip (Fig. 1c). Note that during the deposition process, a very small amount of Au could be deposited on the surface of the cantilever beam, which increased the spring constant of the beam. We roughly estimated this by mechanical analysis. The result showed that, when $5\,\mathrm{nm}$ Au was homogeneously deposited on the cantilever beam (which had cross-section dimension of ~550 nm) and assuming that the Young's modulus of Au was the same as that of SiN (which would definitely generate an overestimation of the influence), the cantilever spring constant would increase by no more than 3.7%
- 4. After Au deposition, the back of the AFM chip was pasted, using silver glue, onto an Au rod, which was then loaded onto the fixed side of a Nanofactory scanning transmission microscope (STM) holder. The polycrystalline nature of the deposited Au offered the opportunity to find an asperity with the 'desired' orientations (for example, the Au asperity has a $<1\bar{1}0>$ axis perpendicular to the AFM cantilever beam and a {111} surface facet parallel to the edge of the AFM tip (Fig. 1d).

W probe preparation. A W tip with an orientation desirable for the friction tests was prepared sequentially, as follows:

- Commercially available W rods with a 99.99 wt% purity (from ESPI Metals)
 were used for this study. The W rod was electrochemically etched into W tips
 at one end (see He et al.56 for the etching method). The tips were normally
 single crystalline, and were dried in air after rinsing sequentially with
 de-ionized water and ethanol alcohol.
- Using TEM, we checked the multiple W rods and found one with the desired tip orientation such that the [110] direction of the tip was parallel to the axial direction of the rod. Then, the W tip was bent into an 'L' shape.
- 3. Thereafter, a W rod with an L-shaped tip was loaded on the piezo-end of the Nanofactory STM holder; driven by the piezosystem of the holder, the W tip was contacted with a clean W rod. Then, an electric pulse was applied to melt quench the tip region; thereafter, the tip had a clean and flat (110) surface.

In situ friction test procedures. The set-up for in situ friction tests in TEM is shown in Fig. 1 and was carried out in following steps:

- The as-prepared AFM-Au cantilever was loaded on the fixed-side of the Nanofactory STM holder; the as-processed L-shaped W tip was attached to the piezo-side of the Nanofactory-STM holder.
- 2. Initially, the orientation of the AFM-Au cantilever was adjusted, by tilting the TEM goniometer, such that the $[1\bar{1}0]$ axis of the Au asperity (with the desired orientations) was parallel to the TEM electron beam, and that the (111) surface of the Au crystal was edge-on and parallel to the AFM tip (Fig. 1b,c).
- Thereafter, the orientation of the W probe was adjusted such that the [001] axis of the W crystal on the tip was parallel to the TEM electron beam and the (110) surface of the W tip crystal was parallel to the (111) surface of the

- Au asperity on the AFM–Au side. For similar orientation control techniques, please refer to the literature⁵⁷.
- 4. Driven by the piezosystem in the Nanofactory STM holder, the W(110) surface was controlled to contact with the Au(111) surface and slide along its [211] or [211] direction at a controlled speed of ~0.1 nm s⁻¹. The normal force on the contact interface was adjusted (both before and occasionally during the tests) by pulling or compressing the W crystal from or against, respectively, the Au asperity, and was kept roughly constant during each friction trial. The in situ friction tests were carried out inside the high vacuum of the TEM (~10⁻⁸ mbar) at room temperature. During the friction tests, the microstructure evolution in the interface vicinity and deflection of the AFM cantilever beam were recorded in real time; then, the friction forces were calculated by Hook's law, that is, by multiplying the deflection and the spring constant (~0.643 nN nm⁻¹) of the AFM cantilever.

Note that the deflection measured from the two-dimensional TEM image was just a projection of its real value in two-dimensions. The error was minimized by keeping the cantilever beam perpendicular to the TEM electron beam and stabilizing the set-up so as to minimize the sample drift during the friction process. However, with high-resolution TEM imaging, the sample drift cannot be avoided totally. Thus, we compared the positions of the cantilever at the starting point of the friction and after being separated with the W probe at the end of the sliding process, and the position difference between the two states was treated as the gross drift of the sample (Au) side. The uncertainty of the determination of the cantilever deflection is mainly from the drift along the sliding direction influenced and the drift along other directions is not considered here. The sample drift was deducted from each frame during analysis by assuming that the drift was at a constant speed and unidirectional on the viewing plane. The drift rate in Fig. 2a-e (the ultralow friction case) was about 0.2 Å s⁻¹ (0.1 Å per frame) and the drift in Fig. 2f-j (the high friction case) was nearly zero. The constant-speed drift was corroborated by the linear movement of the W asperity in the period of interest. The drift rate in our experiments is comparable to the rate in AFM-based experiments (0.01-0.1 nm s⁻¹ for a typical AFM at room temperature)⁵⁸. In such a way, our set-up can provide a rough but reasonable estimation of the friction force. The ratio of the global drift amount to the total cantilever deflection was ~347% at 27 s for the ultralow-friction case in Fig. 2a-e. The drift of the sample under a static state without contact was measured, as shown in Supplementary Fig. 9. Given that the drift is mainly from the thermal drift, the drift rates in contact or without contact are expected to be similar. It was found that the drift without deliberate sliding was nearly linear with the time and the average drift rate was ~0.5 Å s⁻¹, which verified that our assumption about the drift is reasonable.

Molecular dynamic simulation methods. In this study, we performed atomistic MD simulations (as implemented in LAMMPS⁵⁹) to model the friction process at the interface between the W probe and Au surface. The interatomic interaction was described within the formulism of the embedded atom method⁶⁰ for a Au–W binary alloy system parameterized by Zhou et al.⁶¹. In all the MD simulations, the velocity Verlet algorithm with a timestep of 1 fs was used to integrate the equation of motion. The MD simulations were performed in the canonical ensemble, in which the system temperature was maintained at 300 K using the Nosé–Hoover thermostat⁶²

The W probe and Au-surface-treated AFM cantilever were modelled using a supercell that consisted of a rectangular-shaped W slab (2,160 atoms) with a dimension of $5.54\,\mathrm{nm}\times5.15\,\mathrm{nm}\times0.9\,\mathrm{nm}$ and a truncated cone-shaped Au slab (1,079 atoms) with a minimum diameter of $2.74\,\mathrm{nm}$ on top of it in a non-periodic boundary condition along all dimensions. During the MD simulations, the positions of the atoms at the boundary atom layers were fixed, whereas all the other atoms were mobile. Relative to the Au surface, the W probe was first loaded in $0.025\,\mathrm{nm}$ steps at an approaching rate of $0.01\,\mathrm{nm}\,\mathrm{ps}^{-1}$ in the normal direction of the surface. After each vertical loading step, an MD equilibration with a duration of $15\,\mathrm{ps}$ was carried out. When the predestinated vertical position was reached, the W probe was further slid along a direction parallel to the Au surface. During the MD simulation of the sliding process, the modelled system was allowed to equilibrate for $200\,\mathrm{ps}$ every $0.2\,\mathrm{Å}$ travelled by the W probe. The lateral force between the probe and the cantilever surface was calculated to be the friction force.

Density function theory simulation methods. The density functional theory 63,64 calculations were performed within the framework of the projector augmented wave method 65,66 and plane wave basis set, as implemented in the Vienna ab initio package 67-69. The electronic exchange and correlation were evaluated using the generalized gradient approximation in the form of the Perdew-Burke-Ernzernhof functional. A kinetic energy cutoff of 450 eV was adopted for the plane wave expansion. To simulate the formation of a Au layer on a W asperity, a slab that consisted of 42 Au atoms was placed on top of 72 atoms of the W substrate. The distance between the two slabs was set to be 7.3 Å. A single layer of Au was inserted right in the middle of the gap, as is shown in Supplementary Fig. 3i. The positions of top Au layer and bottom W layer were fixed during the structural relaxation. All the atomic positions were optimized until the Hellmann-Feynman force that acted on each atom was less than 0.05 eV Å-1.

Data availability

All data needed to evaluate the conclusions in the Article are present in the Article and/or the Supplementary Information. Additional data related to this Article may be requested from the corresponding authors.

Code availability

The computational code used in this study is available upon request from the corresponding authors.

References

- He, Y. et al. In situ observation of shear-driven amorphization in silicon crystals. Nat. Nanotechnol. 11, 866–871 (2016).
- Zhang, X. et al. Direction-specific van der Waals attraction between rutile TiO₂ nanocrystals. Science 356, 434–437 (2017).
- Ranjan, A., Pey, K. & O'Shea, S. The interplay between drift and electrical measurement in conduction atomic force microscopy. *Rev. Sci. Instrum.* 90, 073701 (2019).
- Plimpton, S. Fast parallel algorithms for short-range molecular dynamics. J. Comput. Phys. 117, 1–19 (1995).
- Daw, M. S. & Baskes, M. I. Embedded-atom method: derivation and application to impurities, surfaces, and other defects in metals. *Phys. Rev. B* 29, 6443–6453 (1984).
- Zhou, X. W., Johnson, R. A. & Wadley, H. N. G. Misfit-energy-increasing dislocations in vapor-deposited CoFe/NiFe multilayers. *Phys. Rev. B* 69, 144113 (2004).
- Hoover, W. G. Canonical dynamics: equilibrium phase-space distributions. Phys. Rev. A 31, 1695–1697 (1985).
- Kohn, W. & Sham, L. J. Self-consistent equations including exchange and correlation effects. *Phys. Rev.* 140, A1133–A1138 (1965).
- 64. Hohenberg, P. & Kohn, W. Inhomogeneous electron gas. *Phys. Rev.* 136, B864–B871 (1964)
- Blöchl, P. E. Projector augmented-wave method. *Phys. Rev. B* 50, 17953–17979 (1994).
- 66. Kresse, G. & Joubert, D. From ultrasoft pseudopotentials to the projector augmented-wave method. *Phys. Rev. B* **59**, 1758–1775 (1999).
- Kresse, G. & Furthmüller, J. Efficiency of ab-initio total energy calculations for metals and semiconductors using a plane-wave basis set. *Comp. Mater. Sci.* 6, 15–50 (1996).

- Kresse, G. & Hafner, J. Ab-initio molecular-dynamics simulation of the liquid-metal-amorphous-semiconductor transition in germanium. *Phys. Rev.* B 49, 14251–14269 (1994).
- Kresse, G. & Hafner, J. Ab initio molecular dynamics for liquid metals. *Phys. Rev. B* 47, 558–561 (1993).
- 70. Perdew, J. P., Burke, K. & Ernzerhof, M. Generalized gradient approximation made simple. *Phys. Rev. Lett.* **77**, 3865–3868 (1996).

Acknowledgements

S.X.M. acknowledges support from National Science Foundation (NSF CMMI 1824816) through the University of Pittsburgh. G.W. acknowledges support from National Science Foundation (NSF CMMI 1662615). C.W. was supported by the PNNL LDRD programme. This work was performed, in part, at the William R. Wiley Environmental Molecular Sciences Laboratory, a national scientific user facility sponsored by US Department of Energy, Office of Biological and Environmental Research and located at PNNL. PNNL is operated by Battelle for the US Department of Energy under contract DE-AC05-76RLO1830.

Author contributions

S.X.M. conceived the experiment. Y.H. carried out the TEM experiments under the direction of S.X.M. and C.W., D.S., Y.H. and X.W. analysed the data. Z.L. and G.W. performed the computational simulations and theoretical analysis. D.S., Y.H., X.W., L.Z. and S.X.M. wrote the manuscript. All the authors contributed to the revision of the manuscript.

Competing interests

The authors declare no competing interests.

Additional information

Supplementary information The online version contains supplementary material available at https://doi.org/10.1038/s41563-021-01091-3.

Correspondence and requests for materials should be addressed to Chongmin Wang, Guofeng Wang or Scott X. Mao.

Peer review information Nature Materials thanks Michael Moseler and the other, anonymous, reviewer(s) for their contribution to the peer review of this work.

Reprints and permissions information is available at www.nature.com/reprints.